Influence of Formic Acid on Electrochemical Properties of High-Porosity Pt/TiN Nanoparticle Aggregates

Takashi Ogi, Ratna Balgis, and Kikuo Okuyama
Dept. of Chemical Engineering, Graduate School of Engineering, Hiroshima University, 1-4-1 Kagamiyama, Higashi-Hiroshima, Hiroshima 739-8527, Japan

Naoko Tajima
Kanomax Japan, Inc., 2-1 Shimizu Suita City, Osaka 565-0805, Japan

Heru Setyawan
Dept. of Chemical Engineering, Faculty of Industrial Technology, Sepuluh Nopember Institute of Technology, Kampus ITS Sukolilo, Surabaya, East Java 60111, Indonesia

DOI 10.1002/aic.14065
Published online March 19, 2013 in Wiley Online Library (wileyonlinelibrary.com)

Platinum-deposited titanium nitride (Pt/TiN) nanoparticle aggregates with high porosities were successfully prepared via a self-assembly-assisted spray pyrolysis method. The addition of formic acid (HCOOH) had a significant influence on the process, promoting the simultaneous formation of metallic Pt and reduction on the surface of the TiN support material. Complete reduction of the Pt/TiN nanoparticle aggregates improved the catalytic activity. The electrochemical surface area (ECSA) of Pt/TiN with HCOOH (Pt/TiN$_{w/HCOOH}$) was 87.15 m^2/g-Pt, which was higher than that of Pt/TiN without HCOOH (Pt/TiN$_{w/o\text{-}HCOOH}$). The catalytic durability of Pt/TiN$_{w/HCOOH}$ was twice that of Pt/TiN$_{w/o\text{-}HCOOH}$. An effective strategy for obtaining carbon-free catalysts with high activities and durabilities was identified. © 2013 American Institute of Chemical Engineers *AIChE J*, 59: 2753–2760, 2013
Keywords: aerosols, catalysis, drying, electrochemistry, nanotechnology

Introduction

The development of new materials for use in polymer-electrolyte fuel-cells (PEFCs) is important. PEFCs have become one of the most promising energy sources because they have advantages such as environmental friendliness and high efficiency. A catalyst support with high-electrical conductivity and good durability is necessary for a PEFC. Carbon black is the most commonly used catalyst support material, as it has desirable characteristics such as high-electronic conductivity and a high-surface area.[1–6] However, the durability of a carbon-based catalyst is relatively low because carbon is thermodynamically unstable under highly acidic PEFC operating conditions.[7,8] Alternative materials with high porosities, high-electronic conductivities, and acid resistance are, therefore, needed to replace carbon supports.

Titanium nitride (TiN) is known to have excellent resistance under acidic conditions. Furthermore, the electronic conductivity of TiN has been reported to be comparable to or even higher than that of carbon black.[9] Recently, Kakinuma et al. succeeded in producing TiN-supported platinum (Pt/TiN) catalyst nanoparticles using an *ex situ* method.[10] The prepared Pt/TiN catalyst had good durability. However, the electrochemical performance was unsatisfactory. In order to increase the electrochemical performance, Pt/TiN was restructured into a packed form using acetylene black, which naturally has an agglomerated structure. This strategy improved the electrochemically active surface area. However, acetylene black itself is a carbon black, and is unstable under acidic conditions, which, therefore, again leads to durability issues. The development of a strategy for producing aggregated Pt/TiN without using carbon black is challenging.

An oxide layer of TiN nanoparticles and incomplete Pt reduction are also reasons for the low-electrochemical performances of Pt/TiN catalysts. As is widely known, the outer surfaces of TiN nanoparticles are easily oxidized, and this influences the interactions of Pt nanoparticles with a TiN catalyst support, and decreases the catalyst activity. However, this issue has not yet been specifically addressed. In this work, the effect of the addition of formic acid (HCOOH) as a reducing agent to the precursor was evaluated in detail. In previous research, we found that HCOOH can efficiently reduce Ni nanoparticle surfaces in spray pyrolysis.[11]

Our group has also reported the effect of catalyst support morphologies on electrocatalytic performances, using a self-assembly-assisted spray pyrolysis method.[12–15] Self-assembly-assisted spray pyrolysis is a promising method for the design of nanostructured particles. This method efficiently produces a dry powder from a nanoparticle sol and precursor solution, and has potential advantages for many applications.[16,17] The

Additional Supporting Information may be found in the online version of this article.

Correspondence concerning this article should be addressed to T. Ogi at ogit@hiroshima-u.ac.jp.

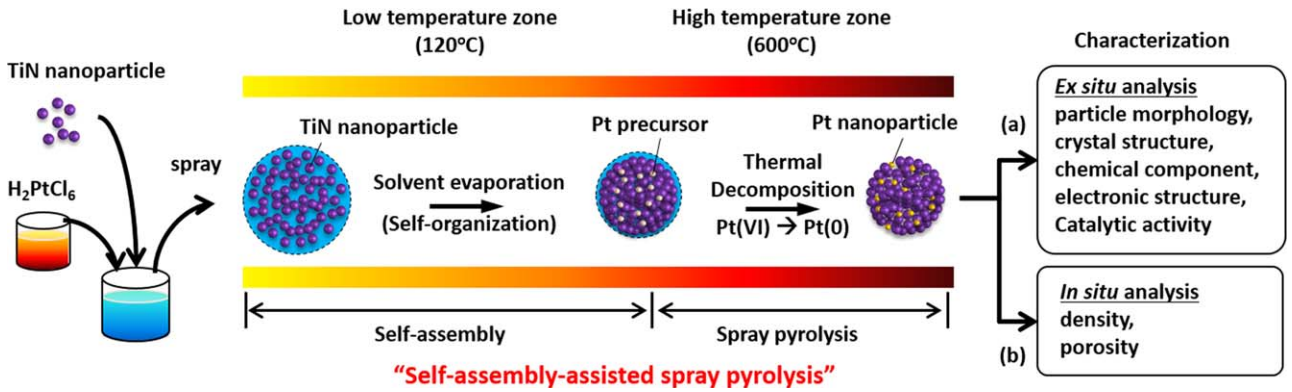

Figure 1. Overall experimental procedure for synthesis of Pt-deposited TiN aggregates by self-assembly-assisted spray pyrolysis.

[Color figure can be viewed in the online issue, which is available at wileyonlinelibrary.com.]

obtained nanoparticle aggregates are on the submicrometer scale, and are easier to handle than nanoparticles. In particular, submicrometer- or micrometer-scale catalysts with controlled morphologies give better transport of reactants and products from the active catalytic sites to the bulk of the fluid than is obtained with nanometer-scale catalysts.

Based on this background, in this article, we describe self-assembly-assisted spray pyrolysis for the preparation of Pt/TiN nanoparticle aggregate catalysts with high porosities. The porosities and densities of the TiN nanoparticle aggregates were measured by *in situ* aerosol technology using a differential mobility analyzer (DMA) and aerosol particle mass (APM) analyzer system. To the best of our knowledge, this is the first examination of the physical properties of TiN nanoparticle aggregates in suspension. Given the important role that such particles play in many industrial materials applications, we believe that the evaluation of the physicochemical properties of nanoparticle materials is of great importance.

Experimental

Figure 1 shows the overall experimental procedure for the synthesis of Pt-deposited TiN (Pt/TiN) nanoparticle aggregates by self-assembly-assisted spray pyrolysis. Details of the procedure are as follows (1) TiN nanoparticles were mixed with an $H_2PtCl_6{\cdot}6H_2O$ precursor solution, (2) the obtained solution was sprayed using an ultrasonic nebulizer, (3) the generated droplets were introduced into a multistage furnace for self-organization of the TiN nanoparticles, followed by thermal decomposition of the Pt precursor for Pt nanoparticle deposition on the TiN nanoparticle aggregates, and (4) the synthesized particles were collected using an electrostatic precipitator in order to determine their particle morphologies, crystal structures, chemical components, electronic structures, and catalytic activities as shown in Figure 1a. The densities and porosities of the synthesized nanoparticle aggregates were also investigated by *in situ* aerosol technology using a DMA-APM system, as shown in Figure 1b.

Preparation of Pt/TiN catalyst

TiN nanoparticles synthesized using a plasma process (Nishin Engineering, Inc., Tokyo, Japan) and an $H_2PtCl_6{\cdot}6H_2O$ dispersion were used as the starting solution. All of chemical materials used in this work were dispersed in ultrapure-water. The Pt/TiN nanoparticle aggregates were synthesized using a self-assembly-assisted spray pyrolysis process. The spray pyrolysis apparatus consisted of an ultrasonic nebulizer (1.7 MHz, NE-U17, Omron Healthcare Co., Ltd., Kyoto, Japan) for droplet generation and an electrical tubular furnace that had two temperature zones, namely 120 and 600°C, as shown in Figure 2.[18] In the low-temperature zone, the solvent evaporated from the droplets, generating a composite of TiN nanoparticles and Pt ions (Pt precursor). In the high-temperature zone, the Pt ions were reduced. The precursor contained a mixture of a 0.5 wt % TiN nanoparticle dispersion solution and an 8.0 wt % $H_2PtCl_6{\cdot}6H_2O$ dispersion; the theoretical amount of added Pt was 20 wt %, based on TiN, and was used in the generation of Pt/TiN nanoparticle aggregate samples without HCOOH, denoted by $Pt/TiN_{w/o\text{-}HCOOH}$. The samples with HCOOH, denoted by $Pt/TiN_{w/HCOOH}$, were obtained by adding 0.6 wt % HCOOH, based on the TiN dispersion solution, to the precursor. HCOOH was used to simultaneously reduce the oxygen bonded on the TiN surfaces and Pt ions to Pt nanoparticles.

Density and porosity characterization

The porosities of the TiN nanoparticle aggregates were obtained from density measurements. The prepared aggregates were directly passed through a density measurement system. This system consisted of a DMA (Model 3081, TSI, Inc., Minneapolis, USA), an APM (Model 3600, Kanomax, Inc., Osaka, Japan) and a condensation particle counter (Model 3022, TSI, Inc., Minneapolis, USA), as shown in Figure 2. The function of the DMA and APM were explained in our previous work.[19] The DMA classifies the particles according to their electrical mobilities Z_p. The relationship between the electrical mobility and mobility equivalent diameter of a particle d_p, is given by the following equation

$$Z_p = \frac{neC_C}{3\mu d_p} \tag{1}$$

where n is the number of elementary charges per particle, e is the unit electrical charge, C_C is the Cunningham slip correction factor, and μ is the gas (nitrogen) viscosity. The mobility equivalent particle diameter of a spherical particle is the same as the diameter of the particle.

The APM classifies particles based on the mass-to-charge ratio.[20] The system consists of two rotating coaxial cylindrical electrodes, with outer and inner radii of 52 and 50 mm, respectively, and a length of 250 mm. The coaxial cylindrical electrodes rotate at the same angular velocity ω. A

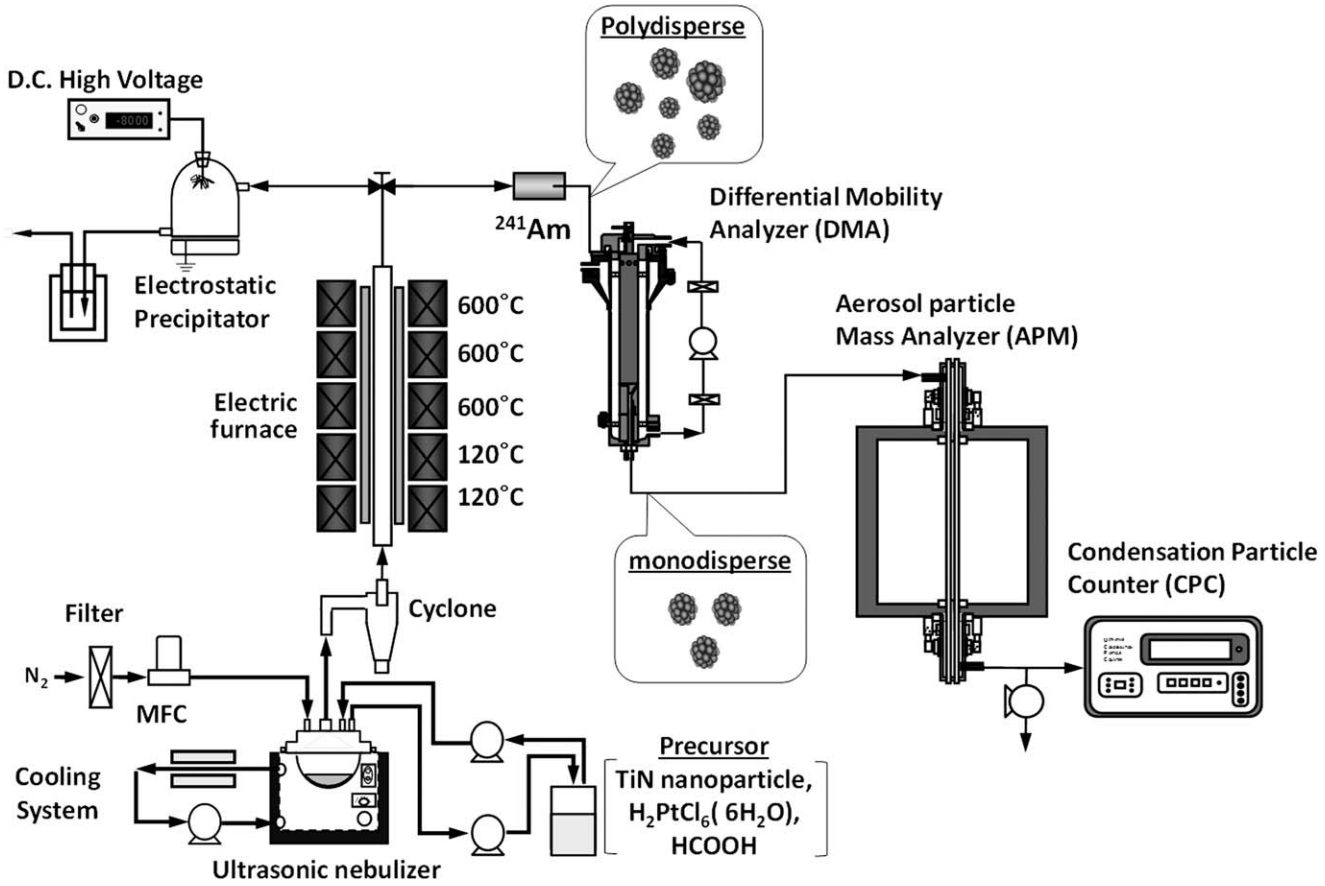

Figure 2. Schematic diagram of the experimental setup.

voltage V, is applied between the electrodes where the particles pass through. The properties of this method, such as sensitivity or accuracy depend on the voltage and angular velocity of the electrodes. The particles are classified by balancing the centrifugal and electrostatic forces. When these forces are equal, particles will penetrate through the rotating cylinders to the downstream detector. The balance between the forces can be described by the following equation

$$m\omega^2 r = neE_{APM} = neV/r\ln(r_1/r_2) \tag{2}$$

where m is particle mass, ω is the APM rotational speed, r is the center radius, and E_{APM} is the magnitude of the electric field in the annular gap (r_1 and r_2).

The effective particle density, ρ, is obtained from both the electrical mobility equivalent diameter d_p, measured by the DMA, and the mass m, measured by the APM, using the following equation

$$\rho = m/\left(\pi d_P^3/6\right) \tag{3}$$

TiN nanoparticle aggregates of dia. 350 nm, classified using the DMA, were introduced into the APM to obtain their densities. The particle porosity is defined as the pore space in a particle, and can vary from 0 to 100%. The particle porosity is stated as

$$\varphi = 1 - \frac{\rho}{\rho_{true}} \tag{4}$$

where ρ is the effective density of the generated particles, measured using the DMA-APM method, and ρ_{true} is the true density of the dense particles.

Catalyst porosity is one of the most important factors in electrocatalytic performance. The higher the catalyst porosity is, the better the three-boundary phase among the catalyst, gas phase, and electrolyte will be. This permeable layer allows effective gas/water diffusion and proton/electron transport to and from the catalytic sites. Although, nitrogen adsorption/desorption is the method commonly used to measure particle density, a large amount of sample is necessary for measurements using this method, and this is a problem when dealing with small rate of samples production. Measurements of particle effective densities using the DMA-APM method, which only needs a small amount of sample and can be performed in situ, is preferable for particles prepared by some methods. If the theoretical density of the particle is known, the particle porosity can be calculated using Eq. 4.

Pt/TiN material characterization

The morphologies of the catalyst particles were observed using field-emission scanning electron microscopy (FE-SEM; Hitachi, S-5000, 20 kV) and transmission electron microscopy (TEM; JEOL-JEM-2010, 200 kV). TEM observations were also used for chemical mapping of catalyst particles, which shows the elements contained in the particles and their dispersion patterns. The electronic structures of the TiN nanoparticles were observed using X-ray absorption fine-structure (XAFS) spectroscopy. Measurements were conducted at the BL27SU line in the Japan Synchrotron Radiation Research Institute (JASRI) in Hyogo, Japan. The crystal structures were determined using X-ray diffraction (XRD,

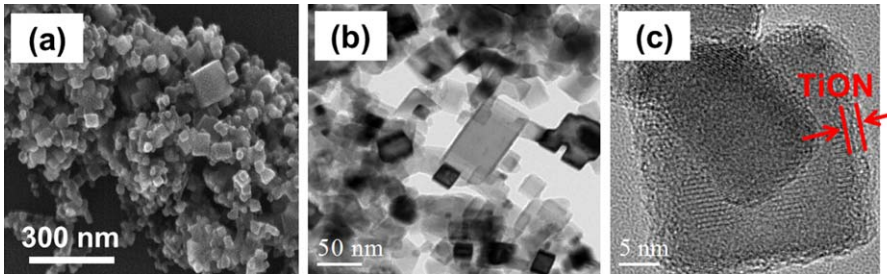

Figure 3. (a) SEM image, (b) TEM image of TiN nanoparticles, and (c) HR-TEM image of single-crystal TiN nanoparticles.

[Color figure can be viewed in the online issue, which is available at wileyonlinelibrary.com.]

Rigaku, RINT2000). The Pt contents in the catalysts were measured using inductively coupled plasma-mass spectrometry (SII, SPS-3000).

Electrochemical characterization

Electrochemical characterizations of the prepared catalysts were performed using cyclic voltammetry (CV) and rotating disk electrode (RDE) measurements (Hokuto-denko, HR-301). Catalyst ink was prepared using the procedure reported elsewhere.[12] The required amount of catalyst ink was transferred to a polished glassy carbon disk ($Ø = 5$ mm, geometric area $= 0.196$ cm^2) and dried to form a thin catalyst layer. The amounts of Pt on the glassy carbon were 7.5 and 5.6 μg-Pt/cm^2 for the Pt/TiN catalysts without and with the addition of HCOOH, respectively. The measurements were performed at room temperature ($\sim$25°C) using a freshly prepared 0.1 M $HClO_4$ electrolyte solution (Cica-reagent, Kanto Chemical Co., Inc., Japan). A nitrogen gas flow at 100 mL/min was passed through the electrolyte solution for 30 min before each CV measurement to deoxygenate the environment. The CV measurements were obtained by scanning between 0 and 1.2 V vs. RHE with a sweep rate of 100 mV/s. The saturating gas was switched to oxygen for the RDE measurements, and the electrolyte was saturated using the same conditions as those for the CV measurements. The rotation rates were controlled at 400, 900, 1600, 2500, and 3600 rpm to collect data for Koutecký−Levich plots. Measurements were carried out at 10 mV/s sweep rates in a typical polarization program of 0.2 V $\rightarrow$ 1.2 V. The background current was measured by running an oxygen-reduction reaction (ORR) sweep profile, without any rotation, in nitrogen-gas-purged 0.1 M $HClO_4$ before the ORR measurement to eliminate any contributions from capacitive current.

Results and Discussion

Measurements of density and porosity using DMA-APM system

The FE-SEM and TEM images in Figure 3a–c show the morphological structure of the TiN nanoparticles. It can be seen that the TiN nanoparticles are cubic and of size around 40 nm; aggregate particles are formed from these nanoparticles. The cubic shape of the primary particles results in a lot of space between particles in the aggregated form; therefore, the aggregates have high porosity. The high-magnification TEM image in Figure 3c shows the appearance of amorphous areas on the particle surfaces, indicating that the TiN surfaces were oxidized, forming TiON.

The FE-SEM image of monodispersed TiN particle aggregates classified as 350-nm particles using DMA is shown in Figure 4. The obtained aggregates were spherical although they consisted of cubic primary particles. This figure also shows the plots of APM outlet concentration as a function of response voltage. The APM rotational speed was kept constant at 1500 rpm, and the peak response voltage that corresponded to the maximum APM outlet concentration of the 350 nm TiN particles was 458.0 V. This voltage corresponds to a measured density of 1292.2 kg/m^3, calculated using Eqs. 2 and 3. The measured density of the TiN nanoparticle aggregates was much less than that of the theoretical (bulk) density of TiN, 5400 kg/m^3, which indicates that in the TiN nanoparticle aggregates, there are many empty spaces among the primary particles. The porosity of the aggregate particles, calculated using Eq. 4 was 76.21%.

Figure 5 shows XAFS spectra of TiN and TiO_2 samples. Unlike other analytical methods, XAFS analysis can detect specific elements in the particle surface and the bulk form, and these are shown as a total electron yield Figure 5a and b and fluorescence yield (Figure 5c and d), respectively. The Ti 2p XAFS spectra of a TiN sample in the surface and in the bulk are shown in Figure 5a and c. TiO_2 particles were also investigated under the same conditions to examine the oxidation level of the TiN sample. The spectra show a complex structure split by a spin-orbit interaction of the Ti 2p levels, with two main features around 460 and 465 eV. The spectrum of the TiN surface shows rather sharp structures similar to those of the TiO_2 spectra; these are characteristic of transition-metal oxides with large intra-atomic interactions. This provides evidence of the formation of TiO_2 on the surfaces of the TiN nanoparticles. The Ti 2p XAFS spectrum of bulk TiN presents a much broader structure and is

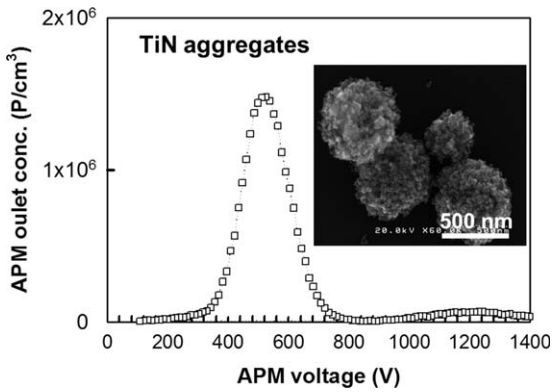

Figure 4. SEM image and APM outlet concentration as a function of response voltage of 350 nm TiN.

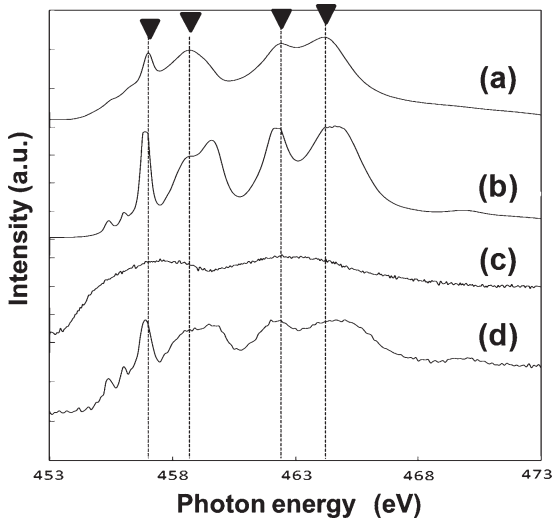

Figure 5. XAFS spectra of TiN and TiO_2 samples: total electron yield analysis (a) TiN sample, (b) TiO_2 sample; fluorescence yield analysis (c) TiN sample, and (d) TiO_2 sample.

different from that of the TiO_2 spectrum. This spectrum corresponds to the previously reported spectrum of TiN.[21]

Morphological characteristics of Pt/TiN catalysts

The morphology of the Pt/TiN catalyst prepared with the addition of HCOOH is presented in Figure 6a and b; the figure shows that the prepared catalyst had a spherical aggregate morphology with many pores on the surface. Figure 6c shows the chemical mapping of $Pt/TiN_{w/HCOOH}$; it can be seen that Pt nanoparticles, represented in yellow, were dispersed uniformly on the TiN surface. A detailed examination of the Pt nanoparticle dispersion was performed using TEM, and the image is shown in Figure 7a. The image confirms a homogeneous distribution of Pt nanoparticles of average size 2.15 nm, as shown in the histogram in Figure 7b. In the catalyst formation process, HCOOH addition is the first step in Pt ion reduction and oxygen reduction on the surfaces of the TiN nanoparticles. The completion of Pt ion reduction to Pt nanoparticles was achieved simultaneously with the formation of catalyst particles, using a spray pyrolysis process. Pt nanoparticles are trapped between compacted TiN nanoparticles, inhibiting Pt particle growth. These phenomena explain the formation of well-dispersed and agglomeration-free Pt nanoparticles.

Figure 8 shows the XRD patterns of $Pt/TiN_{w/o\text{-}HCOOH}$ and $Pt/TiN_{w/HCOOH}$. The diffraction peaks of Pt were observed at 39°, 46°, and 68° (2θ), corresponding to the (111), (200), and (220) crystalline planes, respectively (JCPDS Card no. 4–0802), with a face-centered-cubic crystal structure. The XRD patterns also had sharp peaks around 36°, 42°, 61°, 74°, and 78° (2θ), which correspond to the diffraction peaks of highly crystalline TiN. It is clear that the reduction of $H_2PtCl_6{\cdot}6H_2O$, and the oxidized surfaces of TiN by high-temperature spray pyrolysis was achieved under a nitrogen atmosphere. The addition of HCOOH plays an important role in the TiN crystallinity. The TiN crystal intensity obtained with the addition of HCOOH was bigger than those obtained without HCOOH addition. This is because the pre-reduction treatment using HCOOH successfully cleaned the TiN surface, leaving pure TiN particles, and, during XRD characterization, the real Ti and N atoms arrangement in the crystal can be measured without any disturbance from O atoms.

Electrochemical characterization of Pt/TiN catalysts

The electrochemical characteristics of the prepared Pt/TiN catalysts are presented as CV and ORR polarization curves. Figure 9a shows the typical hydrogen adsorption/desorption

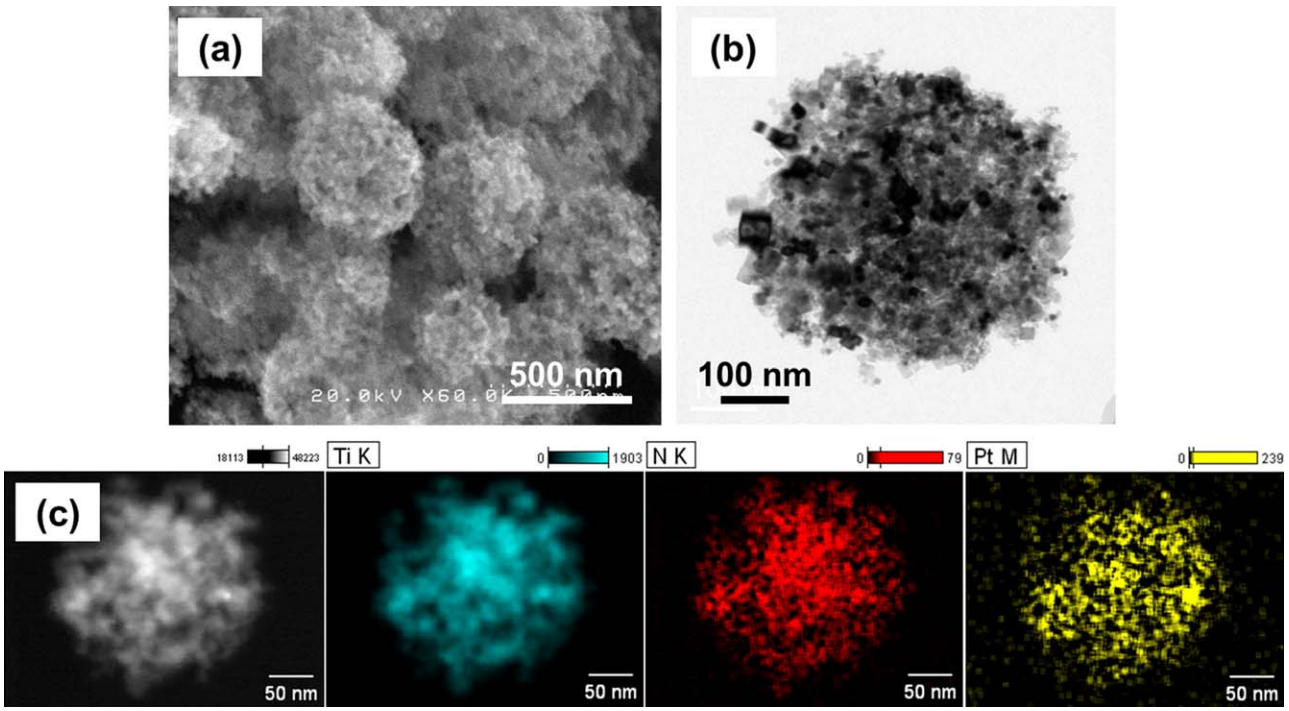

Figure 6. Images of Pt/TiN catalyst aggregate: (a) SEM, (b) TEM, and (c) chemical mapping of Pt/TiN catalyst.

[Color figure can be viewed in the online issue, which is available at wileyonlinelibrary.com.]

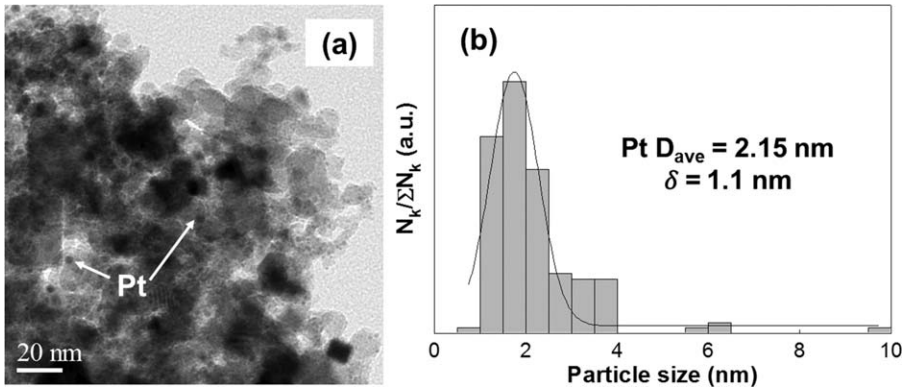

Figure 7. (a) Pt dispersion on TiN surface, and (b) Pt nanoparticle size distribution.

characteristics of Pt/TiN catalysts with and without the addition of HCOOH. The ECSA values of Pt in the working electrode were about 63.51 and 87.15 m^2/g-Pt under the initial condition (10 cycles) for $Pt/TiN_{w/o\text{-}HCOOH}$ and $Pt/TiN_{w/HCOOH}$, respectively, calculated using the hydrogen adsorption charge ($Q_{H\text{-}adsorption}$) area. Both of ECSA value for $Pt/TiN_{w/o\text{-}HCOOH}$ and $Pt/TiN_{w/HCOOH}$ were higher than that of Pt/TiN prepared via liquid phase method (58 m^2/g-Pt) under the initial condition. The ECSA value for $Pt/TiN_{w/HCOOH}$ alone was also higher than that of modified Pt/TiN which was composited with acetylene black (79.2 m^2/g-Pt).[10] The formation of self-assembly Pt/TiN nanoparticle aggregates with its well-developed agglomerate structure could support the electrical conductivity between TiN particles without sacrificing its porosity. More active Pt surface area was presented in this morphology due to the easier access of fuel gas flow through the catalyst.

The durabilities of both prepared catalysts were analyzed up to 1000 cycles, as shown in Figure 9b. Figure 9c shows that the ECSA of $Pt/TiN_{w/HCOOH}$ was more stable than that of $Pt/TiN_{w/o\text{-}HCOOH}$; the total degradation values from 10 to 1000 cycles were 36.7% and 60.9% for $Pt/TiN_{w/HCOOH}$ and $Pt/TiN_{w/o\text{-}HCOOH}$, respectively. The ECSA of $Pt/TiN_{w/o\text{-}HCOOH}$ was lower than that of $Pt/TiN_{w/HCOOH}$ as a result of incomplete Pt reduction, and of oxygen atoms remaining on the TiN surfaces; this accelerates PtO formation and lowers the electrocatalytic activity. The incomplete reduction of Pt ions also decreased the amount of active Pt catalyst, and chloride ions remaining in the catalyst could act as impurities during catalytic activity measurements. This phenomenon explains the low durability of the $Pt/TiN_{w/o\text{-}HCOOH}$ catalyst, which was twice as low as that of $Pt/TiN_{w/HCOOH}$.

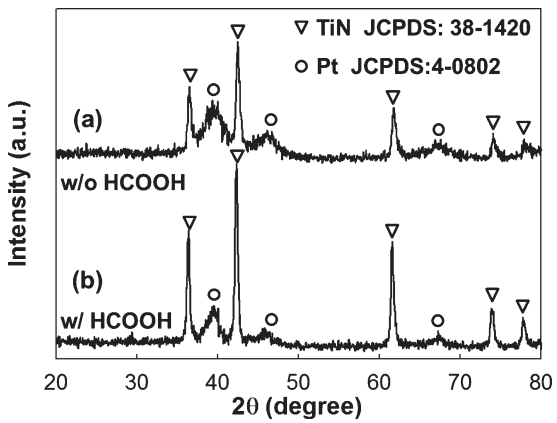

Figure 8. XRD patterns for Pt/TiN catalysts: (a) without HCOOH, and (b) with HCOOH.

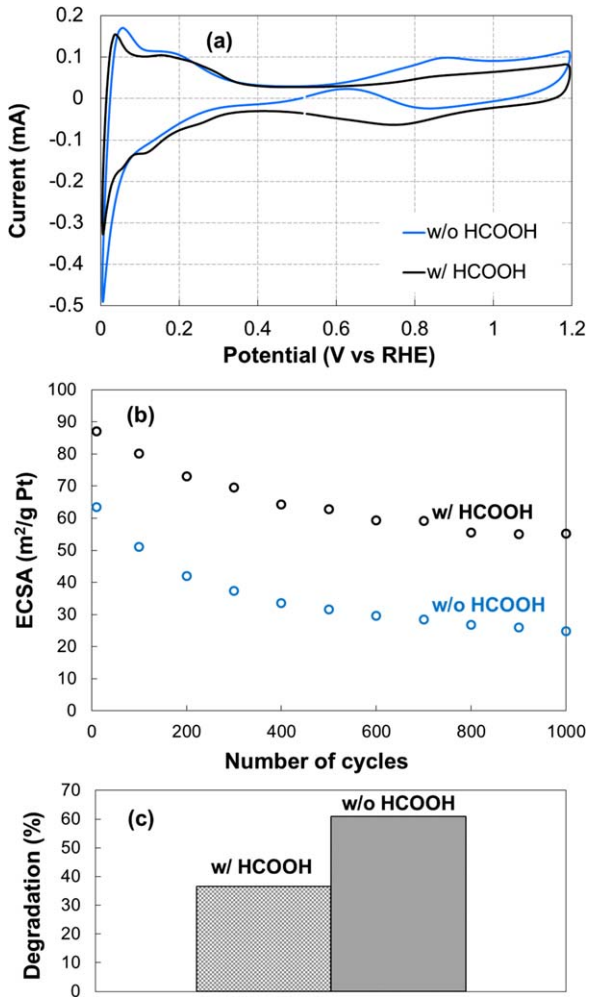

Figure 9. (a) Cyclic voltammograms of Pt/TiN catalysts with and without HCOOH, for 10 cycles in oxygen-free 0.1 M $HClO_4$ (cycling between 0 and 1.2 V at 100 mV/s sweep rate), (b) change in ECSA as a function of number of cycles, and (c) ESCA degradation rates for catalysts.

[Color figure can be viewed in the online issue, which is available at wileyonlinelibrary.com.]

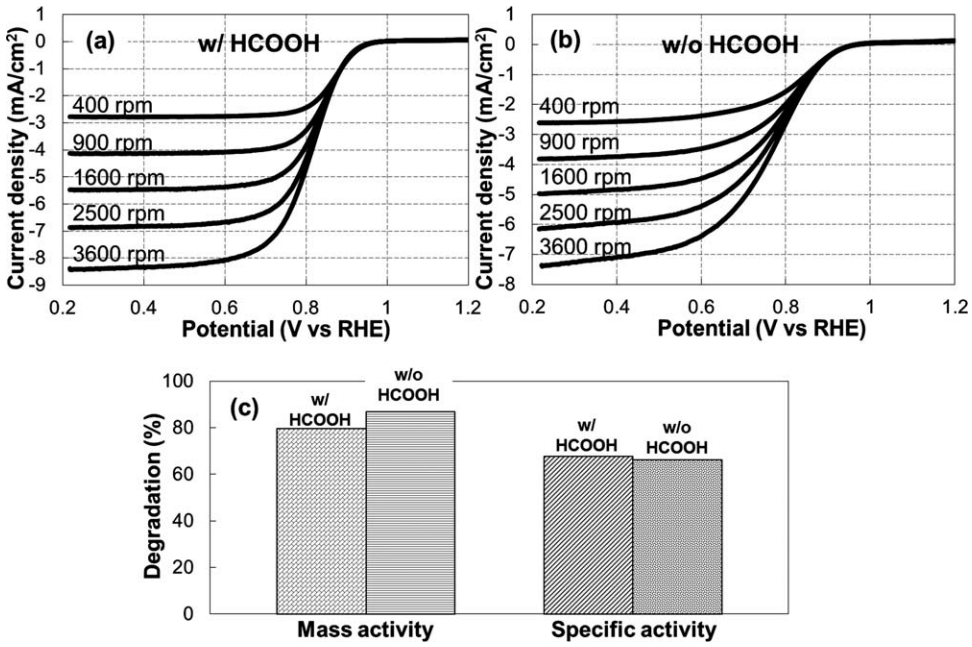

Figure 10. ORR polarization curves at different rotation rates for (a) $Pt/TiN_{w/HCOOH}$, (b) $Pt/TiN_{w/o\text{-}HCOOH}$ in oxygen-saturated 0.1 M $HClO_4$ at a sweep rate 10 mV/s, and (c) degradation rate of mass and specific activities of catalysts at 0.85 V (vs. RHE).

However, it should be noted that the appropriate amount of HCOOH is a requirement which can only be used to enhance the electrocatalytic activity. Figure S1 (Supporting Information) shows the enhancement of CV polarization curve with the increase of HCOOH concentration from 0.15 wt % to 0.6 wt %. However, further increment of HCOOH concentration, up to 1.8 wt %, leads to the extreme degradation of catalyst performance. High amount of HCOOH increases the precursor acidity, which results in some TiN nanoparticle agglomeration and sedimentation in a precursor. This aggregated TiN nanoparticle cannot be sprayed, and the concentration of TiN nanoparticle in the droplet is decreased. As a result, during reduction process, the Pt nanoparticles tend to agglomerate on the surface of small size of TiN nanoparticle aggregates, due to the smaller surface area. It shows that the optimum concentration of HCOOH for enhancing the electrocatalytic performance was existed.

The ORR polarization curves of $Pt/TiN_{w/HCOOH}$ and $Pt/TiN_{w/o\text{-}HCOOH}$ recorded at different rotational speeds are shown in Figure 10a and b, respectively; these were used to obtain Kouteckỳ-Levich plots. The target potential for the calculation of the mass activity and specific activity was $E = 0.85$ V. The mass activity and specific activity were evaluated from the Kouteckỳ-Levich plots using the limiting current method. The Pt mass activity values were calculated by normalizing the Pt loading of the disk electrode, and the specific activity values were estimated by calculating the mass-specific activities and normalizing them to the Pt ECSA. The mass activity values of the $Pt/TiN_{w/HCOOH}$ and $Pt/TiN_{w/o\text{-}HCOOH}$ catalysts under the initial conditions (10 cycles) were 496.90 and 224.51 mA/mg-Pt, respectively, whereas their specific activity values were 570.14 and 353.52 $\mu A/cm^2$-Pt, respectively, as summarized in Table 1. The mass and specific activities of the $Pt/TiN_{w/HCOOH}$ catalyst were higher than those of $Pt/TiN_{w/o\text{-}HCOOH}$ after the stability tests (1000 cycles). The ORR currents were degraded by 79.5% and 86.8% for $Pt/TiN_{w/HCOOH}$ and $Pt/TiN_{w/o\text{-}HCOOH}$, respectively, as shown in Figure 10c. From the catalytic performance results, it is clear that the addition of HCOOH has a significant influence on the reduction of Pt ions and the TiN surfaces. Oxide-free TiN surfaces enhance the electrocatalytic performance. This investigation clearly indicates that the design/engineering and complete reduction of the catalyst/substrate material are very important in achieving high performance.

Conclusions

This study demonstrated a facile strategy for controlling the morphologies of high-porosity Pt/TiN nanoparticle aggregates and simultaneously reducing Pt ions and oxidized TiN surfaces to increase the electrochemical activity of the catalyst. The addition of HCOOH increases the ECSA of the Pt/TiN catalyst to 87.15 m^2/g-Pt and its durability is twice that of Pt/TiN without HCOOH addition. The combination of simplicity of preparation and excellent electrochemical properties make this a promising method for the preparation of carbon-free catalysts for high-performance fuel-cell applications.

Table 1. Catalyst Characterization Results for Pt/TiN with HCOOH

Sample	Pt loading (wt%)	Pt size (nm)	Pt amount on RDE (μg-Pt/cm^2)	ECSA (m^2/g-Pt)	Mass activity (mA/mg-Pt)
$Pt/TiN_{w/HCOOH}$	15	3	5.6	87.15	496.90
$Pt/TiN_{w/o\text{-}HCOOH}$	19.8	5	7.5	63.51	224.51

Acknowledgment

This research was supported by a Grant-in-Aid for Young Scientists (B) (No. 23760729) and Grant-in-Aid for Scientific Research (A) (No. 22246099) sponsored by the Ministry of Education, Culture, Sports, Science, and Technology of Japan. The authors would like to thank Dr. E. Tanabe from the Hiroshima Prefectural Institute of Industrial Science and Technology for helping with the TEM and chemical mapping analysis, and Mr. T. Shirahama and Mr. Y. Sakamoto for assistance with the experimental work.

Literature Cited

1. Schmidt TJ, Noeske M, Gasteiger AH, Behm RJ, Britz P, Brijoux W, Bonnemann H. PtRu alloy colloids as precursors for fuel cell catalysts a combined XPS, AFM, HRTEM, and RDE study. *J Electrochem Soc*. 1998;145:925–931.
2. Paulus UA, Endruschat U, Feldmeyer GJ, Schmidt TJ, Bonnemann H, Behm RJ. New PtRu alloy colloids as precursors for fuel cell catalysts. *J Catal*. 2000;195:383–393.
3. Wang X, Hsing IM. Surfactant stabilized Pt and Pt alloy electrocatalyst for polymer electrolyte fuel cells. *Electrochim. Acta*. 2002;47:2981–2987.
4. Prabhuram J, Zhao TS, Wong CW, Guo JW. Synthesis and physical characterization of Pt/C nanocatalyst for polymer electrolyte fuel cells. *J Power Sources*. 2004;134:1–6.
5. Wang ZB, Zhao CR, Shi PF, Yang YS, Yu ZB, Wang, WK, Yin GP. Effect of a carbon support containing large mesoporous on the performance of a Pt-Ru-Ni/C catalyst for direct methanol fuel cells. *J Phys Chem C*. 2010;114:672–677.
6. Jiang ZZ, Wang ZB, Chu YY, Gu DM, Yin GP. Ultrahigh stable carbon riveted Pt/TiO2-C catalyst prepared by in situ carbonized glucose for proton exchange membrane fuel cell. *Energy Environ Sci*. 2011;4:728–735.
7. Mitsushima S, Koizumi Y, Uzuka S, Ota K. Dissolution of platinum in acidic media. *Electrochim. Acta*. 2008;54:455–460.
8. Yasuda K, Taniguchi A, Akita T, Ioroi T, Siroma Z. Platinum dissolution and deposition in the polymer electrolyte membrane of a PEM fuel cell as studied by potential cycling. *Phys Chem Chem Phys*. 2006;8:746–752.
9. Avasarala B, Haldar P. Electrochemical oxidation behavior of titanium nitride based electrocatalyst under PEM fuel cell conditions. *Electrochim. Acta*. 2010;55:9024–9034.
10. Kakinuma K, Wakasugi Y, Uchida M, Kamino T, Uchida H, Deki S, Watanabe M. Preparation of titanium nitride-supported platinum catalyst with well controlled morphology and their properties relevant to polymer electrolyte fuel cells. *Electrochim. Acta*. 2012;77:279–284.
11. Wang WN, Itoh Y, Lenggoro IW, Okuyama K. Nickel and nickel oxide nanoparticles prepared from nickel nitrate hexahydrate by a low pressure spray pyrolysis. *Mater Sci Eng B*. 2004;111:69–76.
12. Balgis R, Anilkumar GM, Sago S, Ogi T, Okuyama K. Nanostructured design of electrocatalyst support materials for high-performance PEM fuel cell application. *J Power Sources*. 2012;203:26–33.
13. Balgis R, Anilkumar GM, Sago S, Ogi T, Okuyama K. Rapid in situ synthesis of spherical microflower Pt/C catalyst via spray pyrolysis for high performance fuel cell application. *Fuel Cells*. 2012;12(4):665–669.
14. Balgis R, Iskandar F, Ogi T, Purwanto A, Okuyama K. Synthesis of uniformly porous NiO/ZrO2 particles. *Mater Res Bull*. 2011;46:708–715.
15. Balgis R, Anilkumar GM, Sago S, Ogi T, Okuyama K. Ultrahigh oxygen reduction activity of Pt/nitrogen-doped porous carbon microspheres prepared via spray-drying. *J Power Sources*. 2013;229:58–64.
16. Pratsinis SE, Vemury S. Particle formation in gases: a review. *Powder Technol*. 1996;88:267–273.
17. Pratsinis SE. Aerosol-based technologies in nanoscale manufacturing: from functional materials to devices through core chemical engineering. *AIChE*. 2010;56:3028–3035.
18. Iskandar F, Lenggoro IW, Kim TO, Nakao N, Shimada M, Okuyama K. Fabrication and characterization of SiO2 particles generated by sparay method for standards aerosol. *J Chem Eng Jpn*. 2001;34:1285–1292.
19. Lee SY, Widiyastuti W, Tajima N, Iskandar F, Okuyama K. Measurement of the effective density of both spherical aggregated and ordered porous aerosol particles using mobility- and mass-analyzers. *Aerosol Sci Technol*. 2009;43:136–144.
20. Ehara K, Hagwood C, Coakley KJ. Novel method to classify aerosol particles according to their mass-to-charge retio-aerosol particle mass analyser. *J Aerosol Sci*. 1996;27:217–234.
21. Soriano L, Abbate M, Fuggle JC, Prieto P, Jimenez C, Sanz JM, Galan L, Hofmann S. Thermal oxidation of TiN studied by means of soft X-ray absorption spectroscopy. *J Vac Sci Technol A*. 1993;11:47–51.

Manuscript received Dec. 14, 2012, and revision received Jan. 27, 2013.